J. Fluid Mech. (1984), *vol.* 143, *pp.* 277–304
Printed in Great Britain

Structure of a high-Reynolds-number turbulent wake in supersonic flow

By J. P. BONNET, V. JAYARAMAN† AND T. ALZIARY DE ROQUEFORT

Laboratoire d'Etudes Aérodynamiques et Thermiques, Laboratoire Associé au C.N.R.S. 191,
Centre d'Etudes Aérodynamiques et Thermiques,
43 Route de l'Aérodrome, 86000 Poitiers, France

(Received 19 October 1983)

An experimental study of a high-Reynolds-number turbulent wake in supersonic flow is performed using space and space–time correlation measurements by means of hot-wire anemometry. The correlations for the streamwise component of the mass-flux fluctuations are given for six stations starting from the trailing edge down to the asymptotic part. The validity of the Taylor's hypothesis is tested, the convection velocities are determined and the downstream evolution of the optimum space–time correlation is given; the frequency spectra are discussed and the integral lengths are analysed. Finally, the three-dimensional isocorrelation surfaces are given at the six test stations and discussed in relation to classical incompressible-flow results. The downstream evolution of the correlations shows that the two sides of the wake are statistically independent near the trailing edge, and a statistical link is gradually established during the wake development. A three-zonal description of wakes generated by fully developed turbulent boundary layers applies as well for mean quantities (velocity, width) as for turbulence correlations. In the near-wake region the overall structure of the isocorrelation curves is close to that observed in turbulent boundary layers in incompressible flows; some low-frequency phenomena are observed in this region. In the latest part of the wake, an asymptotic state is reached for all the correlation characteristics; the final state reached is not explained by the double-roller-eddy model established for lower-Reynolds-number wakes; it appears that wakes generated by fully turbulent boundary layers behave quite differently from initially laminar wakes, and new turbulent structure models for high-Reynolds-number wakes are to be devised.

1. Introduction

In the study of free turbulent shear flows, the wake configuration is interesting for fundamental and for engineering research as well. In this field, two distinct situations can be considered: in the first one, the Reynolds number of the wake-producing body is low enough to ensure laminar boundary layers at the trailing edge; then, the wake is laminar at its beginning and the transition occurs only during the wake development. In the second case, the Reynolds number is sufficiently high to ensure fully turbulent boundary layers at the trailing edge and the wake is turbulent from its birth.

It is clear, from the shadowgraphs taken by Krummins in the wake of a cone at a Mach number of 10, and reported by Laufer (1975), that the two situations lead

† Present address: Aerodynamics Division, N.A.L., Bangalore 560037, India.

to fundamentally different downstream evolutions of the mean characteristics and of the turbulent structure of the wake.

The first configuration described above is classically encountered in the wakes of cylinders at relatively low Reynolds numbers. The fundamental studies of Townsend (1956) and Grant (1958) concern the structure of such turbulent wakes in subsonic flows by means of space correlations obtained by hot-wire anemometry; Grant made an extensive direct study of the nine components of the correlation tensor in the latest (assumed asymptotic) part of the developed turbulent wake. The analysis of his results led the author to describe the turbulent structure of this wake in terms of the now classical 'double-roller-eddy model'; this description was specified more accurately by Payne & Lumley (1967) and Townsend (1970). Conditional sampling, on the other hand, was used by Thomas (1973) in order to investigate the statistical properties of a wake of the same kind.

For higher speeds, and especially for supersonic flows, the published results on the turbulent structures are very scarce. An important contribution concerns the study of an axisymmetric supersonic wake performed by Demetriades (1976) at an external Mach number $M_\infty = 2$; this author measured the intermittency, scales and space–time correlation with space separation in two directions, in the asymptotic part of the wake. Some less extensive studies were performed using correlation methods in the ballistic range by Fox (1968) and Finson (1973); the non-equilibrium axisymmetric near-wake flow was investigated by Gaviglio *et al.* (1977), with emphasis on autocorrelation measurements.

One can notice a surprising lack of experimental data for the second configuration (i.e. wakes initially turbulent). However, this type of flow is of fundamental interest because the wall turbulence existing in the boundary layer must adapt itself to a sudden removal of the wall and has to relax downstream towards a free turbulence state. For a flat plate the geometrical conditions are very simple and the downstream evolution of the wake is a challenging problem. In fact, insofar as only the mean classical characteristics of this kind of flow are concerned (namely defect velocity and wake width), the work of Ramaprian, Patel & Sastry (1982) clearly shows that the downstream evolution can be described as a three-zone pattern downstream of the trailing edge. Then knowledge of the downstream behaviour of the statistical properties of such turbulent wakes should be of great interest for the interpretation of wake development.

On the basis of the current approach of coherent structures of turbulent flows (see e.g. Hussain 1980; Cantwell 1981), several other related problems can be investigated.

(i) What happens to the structures existing in the turbulent boundary layers when they merge at the trailing edge?

(ii) What is the asymptotic state – if there is any – of the turbulent structures?

(iii) Has any wake an 'indelible' memory of the nature of the boundary layers existing at the trailing edge?

The purpose of the present study is mainly to provide some experimental results in this field. The configuration under investigation is a supersonic two-dimensional wake generated by a thin flat plate; the Reynolds number is very high at the trailing edge in order to ensure fully developed turbulent boundary layers. The downstream evolution of space and space–time correlations of the longitudinal component of the mass-flux fluctuations can be described, despite the great difficulties encountered for the measurements in this kind of flow. The experimental facility and apparatus used in this study are presented in §2, where a general description of the downstream behaviour of mean properties previously measured is given. Section 3 is devoted to

the essential experimental results obtained by means of space and space–time correlation measurements; an overall picture of this flow is then proposed as an attempt to provide some conceptual answers to the abovementioned questions.

2. Experimental procedures and basic flow

2.1. *Equipment and experimental procedure*

2.1.1. *Wind tunnel and model*

All experiments are carried out in the 0.15 m × 0.15 m, open-circuit blowdown wind tunnel of C.E.A.T. of Poitiers. The two-dimensional supersonic nozzle gives a freestream Mach number $M_\infty = 1.975$. The total pressure is 6 bar and total temperature is about 250 K, decreasing at a rate of about 0.3 K s^{-1}, the usual running time of the tunnel is 30 s, depending on the kind of measurements to be performed. With these conditions, the freestream unit Reynolds number obtained is 0.96×10^6 cm^{-1}. The freestream turbulence level is 0.4 %, expressed in terms of mass-flux fluctuations (Bonnet 1982).

The model used for the generation of the wake is a steel flat plate, 0.3 cm thick, with leading edge located 5 cm upstream of the sonic throat, where the local Mach number is 0.85; it is 15 cm wide, with a length in the supersonic part of the flow equal to 80 cm, resulting in a Reynolds number of 8×10^7. The trailing edge is bevelled with a 3° double wedge angle and the boundary layers at this location are turbulent with a thickness of about 1 cm.

The X-axis is in the freestream direction, starting at the trailing edge. The Y-axis is normal to the wake plane (the maxima of mean gradients are along the Y-axis); the Z-axis is parallel to the trailing edge of the plate (the mean motion is homogeneous in the Z-direction).

2.1.2. *Measurement techniques*

All the turbulence measurements are obtained with constant-temperature hot-wire anemometers (CTA). The frequency response in phase and amplitude is checked by electric tests and by heating the wire with a modulated laser beam (Bonnet & Alziary de Roquefort 1980). Satisfactory frequency response is obtained up to 500 kHz with a DISA 55M12 symmetrical-bridge anemometer at an overheat ratio of 0.8. Previous measurements have shown that, in the present flow, the useful energetic range lies generally under 300 kHz.

The hot-wire probes used in this study are DISA 55P11 and 55P12 specially modified to avoid spurious vibrations of the supports. The wires of diameter 2.5 μm are made of platinum-plated tungsten and are 0.5 mm long. Each wire and CTA are tested, before use, in a specially designed, small dimensions calibration wind tunnel in order to eliminate the wires giving too high strain-gauge effects and to make the electronic adjustments.

During the runs, the two a.c. output signals of the CTA are recorded using a magnetic-tape recorder (Bell & Howell type M14G) on two FM II channels with 0–500 kHz bandwidth; the d.c. levels and the displacement synchronization signals are recorded on FM I channels (0–80 kHz bandwidth) at a tape speed of 120 in s^{-1}. The usual reproduction speed is 7.5 in. s^{-1}, giving a 16:1 ratio for time dilatation.

2.1.3. *Correlation measurements*

The measurements of space and space–time correlations are made both by analog means using classical devices and by numerical means using a minicomputer. The

hot-wire signals are first used during the run to give direct space correlations and then replayed in order to obtain space and space–time correlations, filtered or not.

Two r.m.s. voltmeters (DISA 55D35), one turbulence processor (DISA 52B25) and a time-delay unit (55D75) are employed to obtain $(\overline{e_1^2})^{\frac{1}{2}}$, $(\overline{e_2^2})^{\frac{1}{2}}$ and $\overline{e_1(t)\,e_2(t+\tau)}$, where $e_{1,2}$ is the output fluctuating voltage of each anemometer, τ being the time-delay imposed between the two signals. Assuming that the correlation coefficient between the two signals is representative of mass-flow fluctuation correlation is a reasonable approximation, which is consistent with a full analysis performed by Demetriades (1976):

$$R = \frac{\overline{e_1(X, Y, Z; t)e_2(X+x', Y+y', Z+z'; t+\tau)}}{[\overline{e_1^2(X, Y, Z; t)}]^{\frac{1}{2}}[\overline{e_2^2(X+x', Y+y', Z+z'; t)}]^{\frac{1}{2}}}$$

$$\approx \frac{\overline{(\rho u)'(X, Y, Z; t)\,(\rho u)'(X+x', Y+y', Z+z'; t+\tau)}}{[\overline{(\rho u)'^2(X, Y, Z; t)}]^{\frac{1}{2}}[\overline{(\rho u)'^2(X+x', Y+y', Z+z'; t)}]^{\frac{1}{2}}}$$

$$\approx R_{11}(x', y', z'; \tau),$$

where ρ is the density and u the longitudinal component of the velocity; the primes denote centred fluctuations and the overbar represents the mean values, with $\overline{(\ )'} = 0$.

In fact, the complete resolution of the mode correlation, which can give correlations for velocity and/or temperature fluctuations, is indeed always possible using several overheat ratios (Morkovin 1956), but very time-consuming. In an axisymmetric supersonic wake, Demetriades (1976) performed a full analysis; comparisons between restored and unrestored correlations show that 'the differences are rather minor and an approximate notion of the most complex feature of the wake turbulence can be obtained by looking at the raw signals' (Demetriades 1976).

The correlation data are obtained during a run by keeping a stationary probe at a coordinate point hereinafter denoted by X, Y and Z, and traversing a second wire located at $X+x'$, $Y+y'$ and $Z+z'$ (changing y' step by step during a run). The two wires are connected to identical CTA; the two anemometers have nearly the same transfer functions, provided that the useful upper frequency limit is low enough. Owing to the low-pass-filtering effect introduced by the space and time differences between the two signals, one can neglect the phase shift between the two records.

In the case of numerical procedures, the recorded signals are digitized and stored on a minicomputer; the sampling frequency, taking into account the speed ratio of the record and reproduce tape speeds, is 330 kHz per channel. The interval between the sampling of each channel introduces an interchannel time delay of 1.56×10^{-6} s, which is taken into account in the numerical procedure. The output signals from the recorder are low-pass filtered below the Shannon frequency with two paired active filters (Schlumberger FAB 24 at 24 dB/octave).

2.1.4. *Basic mean- and turbulent-flow characteristics*

In this subsection we recall some of the basic flow characteristics of the wake under study, carried out by Bonnet (1982), which are essential in understanding the present correlation results.

The two-dimensionality of the mean flow in the wake is found to be satisfactory; measurements show that the mean value of the total temperature is nearly constant inside the wake. The momentum thickness θ remains practically constant and is taken equal to 1.3 mm.

One essential conclusion arising from previous measurements (Bonnet & Alziary

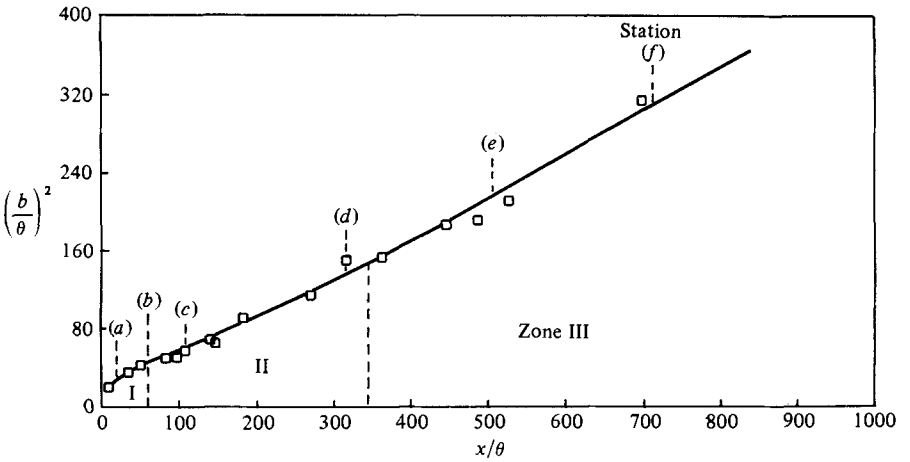

FIGURE 1. Streamwise evolution of the characteristic width of the supersonic wake.

de Roquefort 1983) should be recalled: the mean characteristic of the supersonic wake studied here behaves as in the case of a subsonic wake, provided that the two wakes are created by fully developed turbulent boundary layers. As shown by Ramaprian *et al.* (1982), from the analysis of their experiments and those of Pot (1979), the originally turbulent wake can be described following three distinct regions from the trailing edge. Nearly identical results are obtained in the supersonic wake studied here; from mean-value measurements, namely wake width (denoted by b) and axis mean velocity (denoted by U_0), one can define the three regions starting at the trailing edge: first, the region I, called the near-wake region, which is characterized by a very rapid increase of b and U_0, without any similarity of the profiles; this region is followed by the region II, called the intermediate wake, where the increases of b and U_0 are lower and some qualitative self-similarity exists; in the last part of the wake, region III, called the developed wake, each mean quantity satisfies quantitatively the theoretical similarity-analysis results (Bonnet 1982).

This overall behaviour can be observed in the evolution of the half-defect velocity thickness b plotted in figure 1. The compressibility does not seem to affect this downstream behaviour. However, it appears that the self-preserving state of turbulent profiles, obtained in the last part of the wake (region III), shows some mean Mach-number effects which do not appear in mean-velocity profiles (Bonnet & Alziary de Roquefort 1983).

3. Experimental results

3.1. *General characteristics of the wake at the test stations*

Detailed measurements of space and space–time correlations are obtained at six different downstream positions in the wake, namely $X = 25$, 80.5, 140, 410, 643 and 922 mm, starting from the trailing edge down to the far-wake region; these positions are denoted in figure 1 as stations (a), (b), (c), (d), (e) and (f) respectively. For each station, the measurements are carried out at various values of transverse and lateral positions. For transverse positions the measurements are performed mainly for the values of $Y = 0$, $Y = Y_m$ (and $Y = \frac{1}{2}Y_m$ for some stations), where Y_m is the location of the maximum of fluctuations at each station.

Station (a) is located in the near-wake region (region I), while station (b) is situated

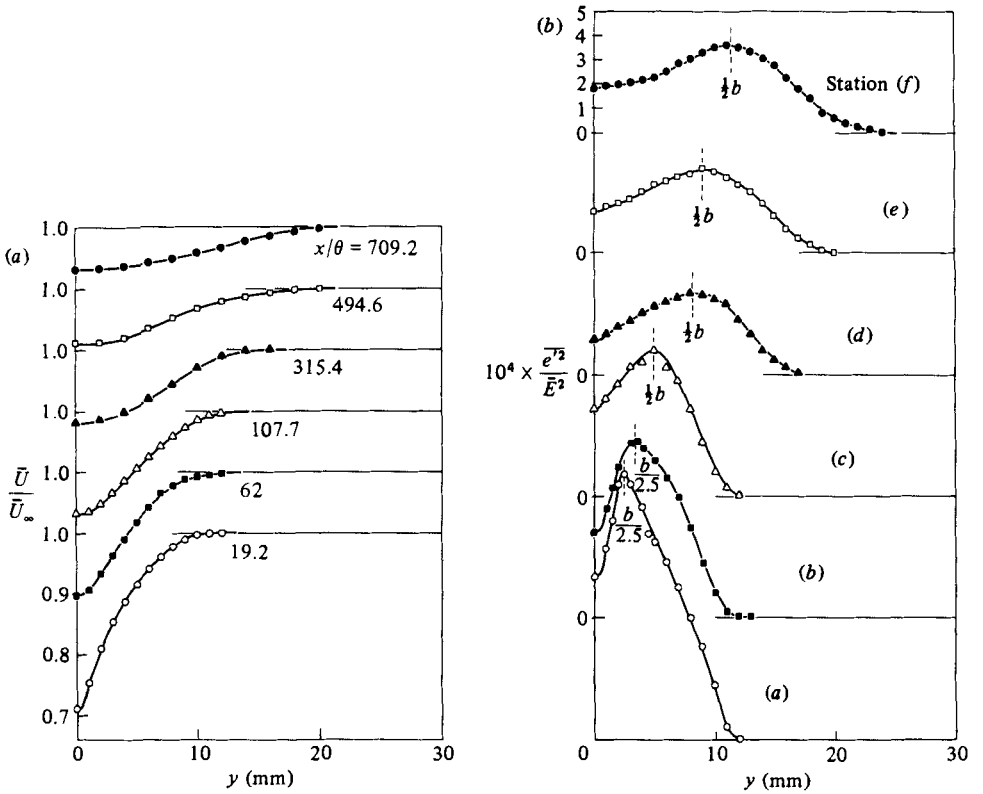

FIGURE 2. Mean characteristics of the supersonic wake. (*a*) Mean-velocity profiles at, or at the vicinity of the tested stations. (*b*) Mean-square values of the CTA anemometer output at the tested stations.

Station	(*a*)	(*b*)	(*c*)	(*d*)	(*e*)	(*f*)
X (mm)	25	80.5	140	410	643	922
X/θ	19.2	60	108	315	492	709
b (mm)	7	8.8	10	16	18	23
b/θ	5.4	6.8	7.8	12.3	13.8	17.7
$(U_\infty - U_0)/U_\infty$	0.29	0.2	0.17	0.12	0.09	0.07

TABLE 1

between regions I and II; station (*c*) corresponds to the main part of the intermediate wake (region II), and the next station (*d*) is between regions II and III. The last two stations, (*e*) and (*f*), are situated in the far wake (region III) (see figure 1).

Figure 2(*a*) shows the distribution of the mean-velocity profiles U/U_∞ (where ∞ refers to freestream conditions) at (or near) the stations where the correlations are measured. Figure 2(*b*) shows the distributions of the fluctuations $\overline{e^2}/E^2$ of the anemometer output, giving the local values of Y_m.

Table 1 gives the overall characteristics of all the stations (U_∞ is the mean velocity in the freestream flow, and the index 0 denotes the axis values); the half-velocity-defect thickness b is defined as $b = |Y_1 - Y_2|$, Y_1 and Y_2 being the ordinates where $U(Y_1 \text{ or } Y_2) = \frac{1}{2}(U_\infty + U_0)$. In the following discussions of the space and space–time

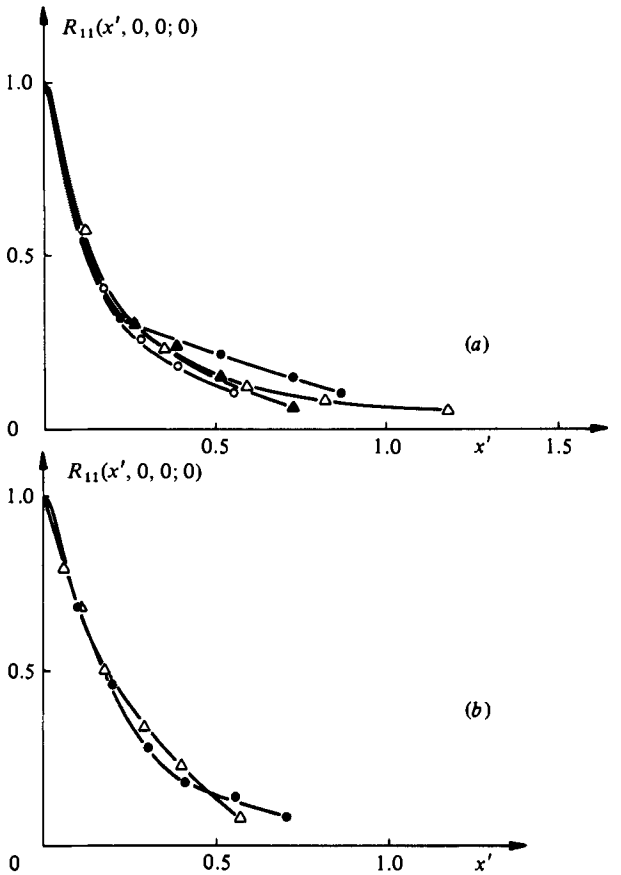

FIGURE 3. Longitudinal space-correlation $R_{11}(x', 0, 0; 0)$. (*a*) On the wake axis: ●, station (*a*); △, (*b*); ▲, (*c*); ○, (*e*). (*b*) Off the wake axis: ●, station (*c*) at $Y = 0.6$; △, (*e*) at $Y = 0.5$.

correlation measurements, the values of space separation are non-dimensionalized by the local value of b. On the other hand, the X-location of each station will be non-dimensionalized by the constant value of the momentum thickness θ.

3.2. *Downstream evolution of space correlation*

3.2.1. *With separation in the mean-flow direction; $R_{11}(x', 0, 0; 0)$*

The measurements of space correlations following the X-axis are performed only for stations (*a*), (*b*), (*c*) and (*e*) with the stationary probe on the axis, and for stations (*c*) and (*e*) with the stationary probe off the axis at the point $Y = Y_m$. All these measurements are obtained by extrapolation of $R_{11}(x', y', 0; 0)$ for $y' \to 0$ in order to avoid errors due to the wake of the upstream probe impinging on the downstream one; some technological constraints limit the extension of the x' domain.

In figure 3(*a*) rather good regroupment of the curves can be observed on the axis of the wake. In figure 3(*b*) it appears that, when the probes are located off the axis, the correlation goes more rapidly towards zero values at station (*c*). However, the limitation of the x' extent does not allow a more precise discussion; the discussion of space–time correlation measurements will later give more precise information concerning this matter for all the stations tested.

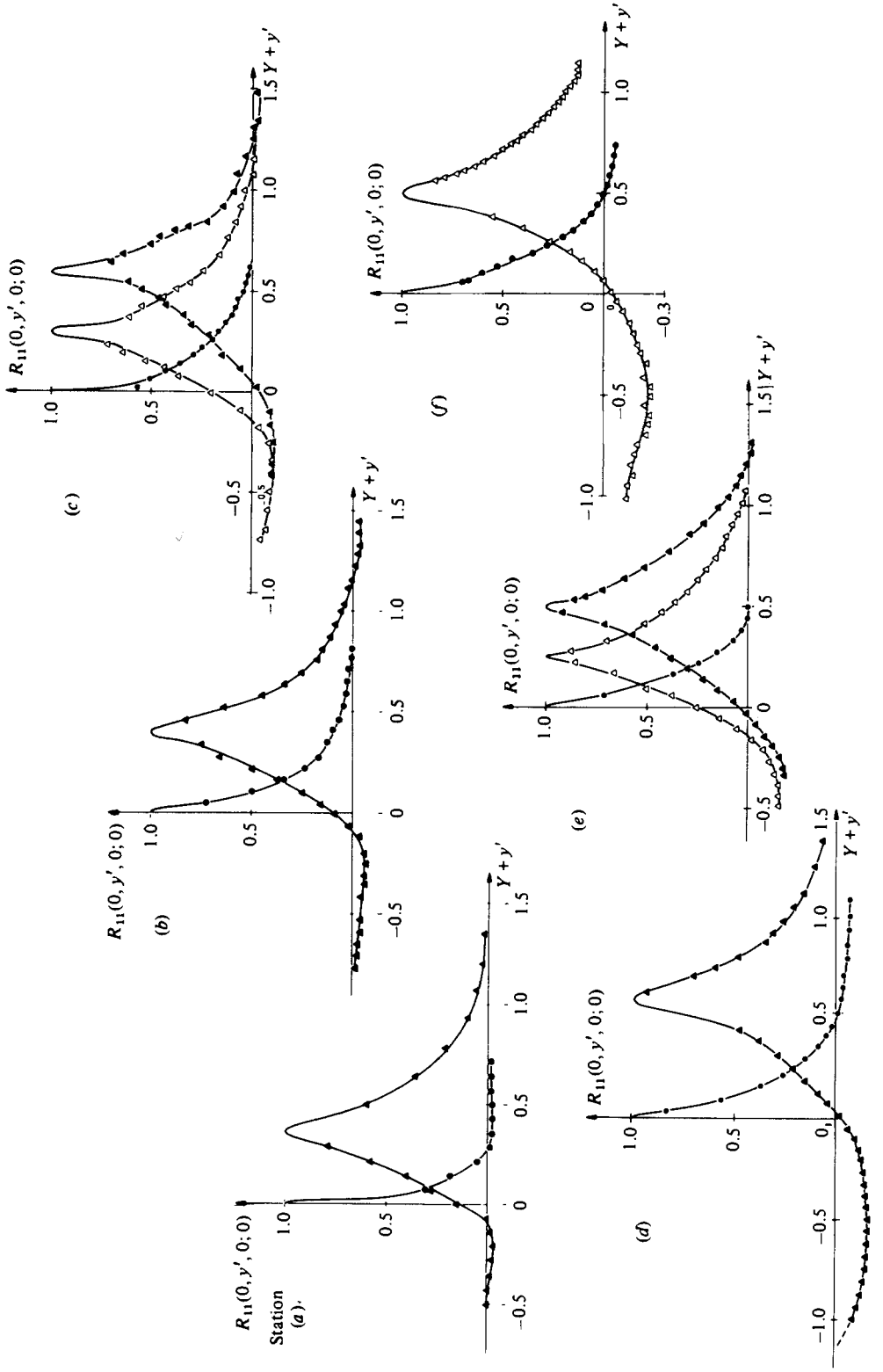

FIGURE 4. Behaviour of the transverse (Y) component of the space correlation $R_{11}(0, y', 0; 0)$. Fixed probe on the wake axis $Y = 0$ (●), at the maximum-fluctuation location $Y = Y_m$ (▲), and at the intermediate location $Y = \frac{1}{2}Y_m$ (△).

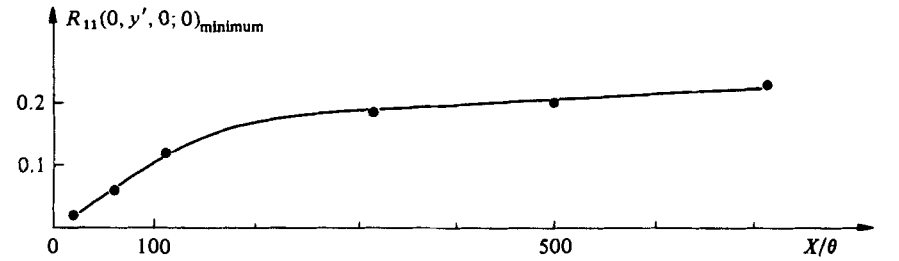

FIGURE 5. Streamwise evolution of the minimum of the space correlation $R_{11}(0, y', 0; 0)$. One probe is located at $Y = Y_m$, the other probe is placed at the symmetrical location relative to the wake axis ($y' \approx -2Y_m$).

3.2.2. *With transverse separation, normal to the wake plane;* $R_{11}(0, y', 0; 0)$

Measurements are performed for each test section and the results are plotted in figures 4(*a*)–(*f*). For this kind of measurement we have to distinguish between the situation where the stationary probe is positioned on the axis (where symmetry considerations should apply for y') and the situation where the probe is off the axis.

(i) *Stationary probe on the wake axis.* The main observation arising from figure 4 is that, at the first station (*a*) near the trailing edge, the correlation reaches zero very near the axis of the wake ($R_{11}(0, y', 0; 0) = 0$ for $y' \approx Y_m$) compared with the value of $y' \approx \frac{1}{2}Y_m$ for the other five stations. However, it should be recalled that b cannot be a good parameter for non-dimensionalization in the near-wake region. The local value of Y_m would be probably a more suitable parameter; however, the ratio of y'/Y_m is equal to 0.7 at the first station (*a*) and about unity for the other stations, so that we can postulate that, near the trailing edge, the relative scales of the correlations are quite different in comparison with the stations located downstream.

(ii) *Stationary probe off the wake axis.* When the stationary probe is located off the wake axis, two cases must be considered: (*a*) the moving probe is displaced towards the outer part of the wake (i.e. $y' > 0$), and, (*b*) the moving probe is displaced towards the axis of the wake (i.e. $y' < 0$).

For $y' > 0$ no fundamental differences between the different test sections can be observed; it appears that $R_{11}(0, y', 0; 0)$ reaches zero for $Y + y' \approx 1.25$ at all positions downstream of the trailing edge, independently of the position of the stationary probe off the axis (figure 4).

For $y' < 0$ one can first observe that the axis of the wake has an important influence. Particularly when the two probes are located on each side of the wake (i.e. $Y + y' < 0$), the value of $R_{11}(0, y', 0; 0)$ becomes more and more significantly negative when the distance from the trailing edge increases: this typical behaviour is observed either for $Y = Y_m$ or for $Y = \frac{1}{2}Y_m$. Figure 5 shows the evolution of the minimum value of $R_{11}(0, y', 0; 0)$ (for $Y + y' \approx -Y_m$) as a function of X when the stationary probe is placed at the point $Y = Y_m$.

It appears clearly from figure 5 that there is a very rapid evolution of this minimum between station (*a*) and station (*c*) which corresponds to $X/\theta < 350$. This behaviour seems to be directly related to the rapid evolution of the mean characteristics of the wake (for example b or U_0/U_∞) between the trailing edge and the beginning of the asymptotic region which occurs for $X/\theta \approx 350$ as previously measured (cf. §2.1.4). The asymptotic state of the mean characteristics and of the correlations seems to be obtained at the same distance from the trailing edge.

Moreover, these results show that a significant statistical relationship between the

two sides of the wake builds up from the trailing edge; one indeed expects that the boundary layers on each side of the flat plate are uncorrelated at the trailing edge and generate two quite independent parts of the initially turbulent wake; when the distance from the trailing edge increases, the two parts of the flow appear to be more and more correlated, reaching a constant level of correlation nearly equal to -0.2; the statistical dependence of the two sides of the wake grows rapidly in the 'developing' wake and is well established in the last stations.

This fundamental characteristic of the correlation between the two sides of the wake in the asymptotic region does not agree with the measurements of Grant (1958) in the incompressible wake, initially laminar, of a cylinder, where there is no evidence of negative values of $R_{11}(0, y', 0; 0)$ whatever the y-separation may be.

This discrepancy between our results and those of Grant can be attributed partly to compressibility effects present only in our study, and, chiefly to the wake generation itself; in the present work, the wake is generated by fully developed turbulent boundary layers, whereas in the work of Grant the wake is created by a rod at such a Reynolds number that the boundary layers are laminar on the rod so that the wake evolves from a laminar one to a turbulent one during its development. We have recalled in §2.1.4 that the downstream behaviour of the mean characteristics of wakes depends strongly on the initial conditions (laminar or turbulent); in particular, the three-zonal description of the increase of the wake width b is quite similar for subsonic and supersonic wakes provided that they are generated by turbulent boundary layers, and very different indeed for initially laminar wakes; the compressibility essentially affects the asymptotic profiles of turbulent quantities. Therefore it seems that the discrepancies observed between our results and those of Grant could be attributed mainly to the own 'history' of the wake, which perhaps never completely forgets its origin.

3.2.3. *With transverse separation parallel to the trailing edge* $R_{11}(0, 0, z'; 0)$

Figure 6 shows the space correlation $R_{11}(0, 0, z'; 0)$ plotted against the Z-separation at different test sections.

From this figure it appears that the effect of increasing the Z-separation between the two probes is quite different near the trailing edge than for downstream. One can observe in the near wake (stations (*a*) and (*b*)), that the correlation coefficient reaches significant negative values and follows a quasi-periodic behaviour when the Z-separation increases; this is true if the two probes are located either on or off the wake axis. At the last three stations this behaviour is no more noticeable. In particular, at the last downstream test section (*f*), no negative values are measured independently of the Z-separation.

The results obtained at the first station seem to be in a qualitative agreement with the measurements of Grant (1958), for example, performed in a turbulent (incompressible) boundary layer. On the other hand, the characteristics shown at the last section are quite different than those observed by Grant in the subsonic wake of a cylinder: the results of this author show that the coefficient $R_{11}(0, 0, z'; 0)$ reaches significant negative values for large Z-separation and for all Y-positions of the probes; this later behaviour led Grant, and later Townsend (1970) and Payne & Lumley (1967), to postulate the existence of counter-rotating eddies, which clearly does not apply to the wake considered here.

The abovementioned fundamental differences between the origins of the wakes observed by Grant and the present study remain valid for the discussion of the $R_{11}(0, 0, z'; 0)$ measurements. Near the trailing edge, the 'memory' of structures

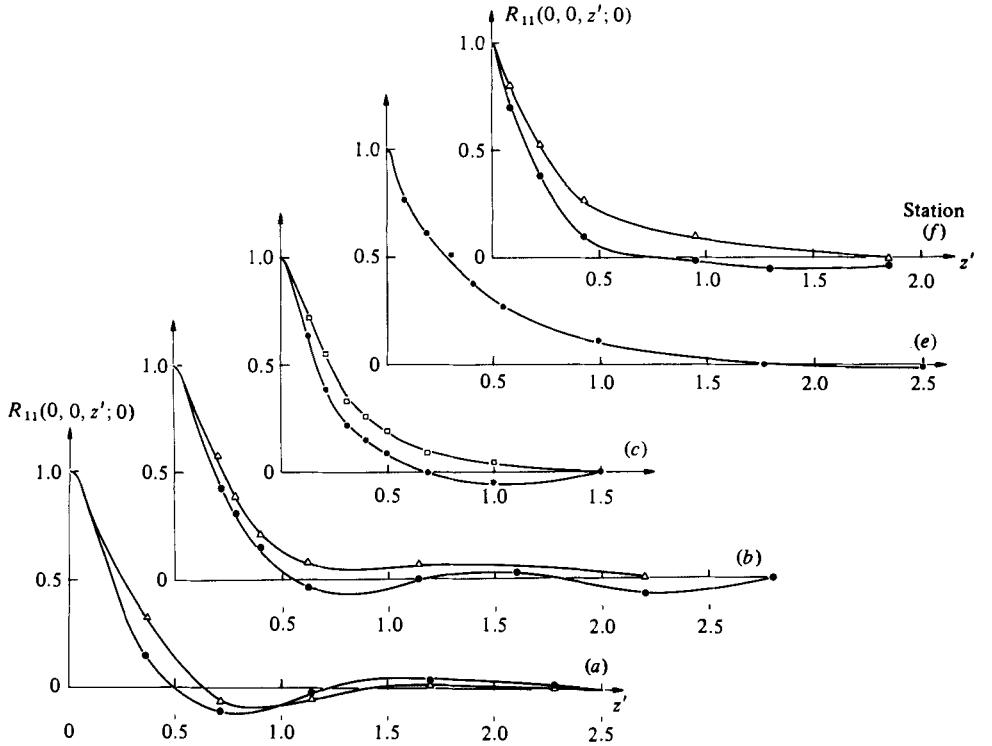

FIGURE 6. Behaviour of the transverse (Z) component of the space correlation $R_{11}(0, 0, z'; 0)$. The two probes are located either on the wake axis (●) or at the maximum fluctuation location $Y = Y_m$ (open symbols).

existing in the boundary layers clearly affects the correlations; gradually, when the distance from the trailing edge increases, another situation takes place and leads to the asymptotic part which cannot be interpreted directly in terms of counter-rotating eddies, as it is the case in the study of Grant.

3.3. *Evolution of the space–time correlation*

Though the method of space-correlation measurements is a powerful way to study turbulent structures, this approach suffers from a number of shortcomings (see Cantwell 1981). An extension of this method is the use of space–time correlation measurements, which has many advantages over the previous technique and can be easily applied to supersonic flows. Usually, this approach gives a deepest understanding of the flow as compared to space correlations. As far as space–time correlations are concerned, the number of results rapidly increases, and, in order to emphasize only the essential facts arising from these measurements, we shall present only a few exanples of the results obtained. More detailed results can be found in Jayaraman (1983).

3.3.1. *Convection velocity*

Following Favre *et al.* (1976), the convection velocity U_c can be obtained by plotting the isocorrelation curves $R_{11}(x', 0, 0; \tau)$ in X and $\tau U_c/b$ coordinates. As an example, from the space–time correlations obtained at station (e), the curves of isocorrelations shown on figure 7 can be plotted. The contour plots looks like very elongated ellipses, so that the three possible determinations of U_c proposed by Favre *et al.* (1976) are

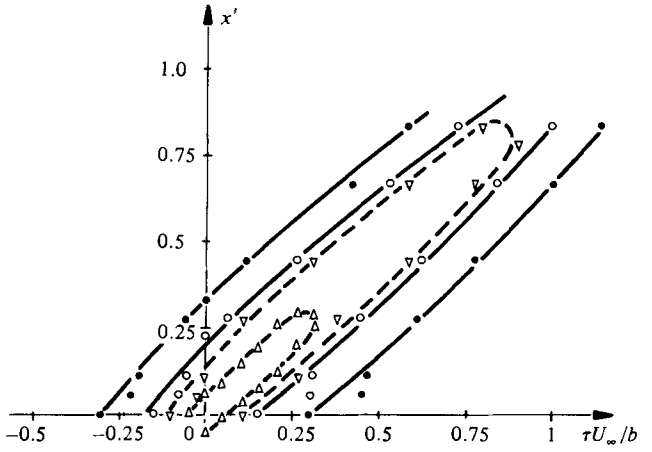

FIGURE 7. Isocontours of the space–time correlation $R_{11}(x', 0, 0; \tau)$ at station (*e*): ●, $R_{11} = 0.3$; ○, 0.5; ▽, 0.6; △, 0.8.

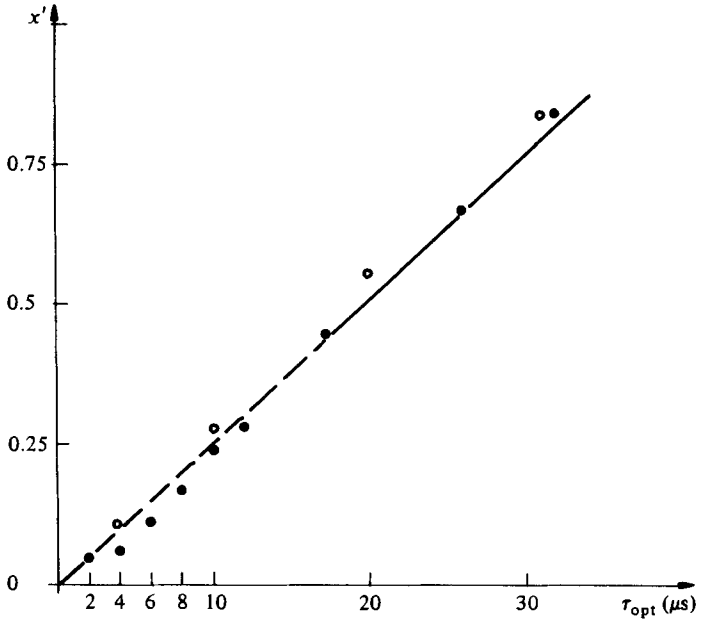

FIGURE 8. Optimum time-delay versus space separation at station (*e*) for $Y = Y_m$ (○) and $Y = \frac{1}{2}Y_m$ (●).

nearly equivalent and lead to $U_c/U_\infty \approx 0.95$; this result is in good agreement with the determination made more directly by plotting the optimum time delay τ_0 (see figure 8), as done for instance by Demetriades (1976) in a supersonic axisymmetric wake. The convection velocity obtained by this author is quite in agreement with our results. The values obtained for all the test sections show that $U_c/U_\infty \approx 0.95$ everywhere except for the first station (*a*) near the trailing edge where $U_c/U_\infty \approx 0.75$.

3.3.2. *Autocorrelation and Taylor's hypothesis*

The autocorrelation measurement is an important tool for the study of turbulence. Provided that Taylor's hypothesis remains valid, some space correlations can be

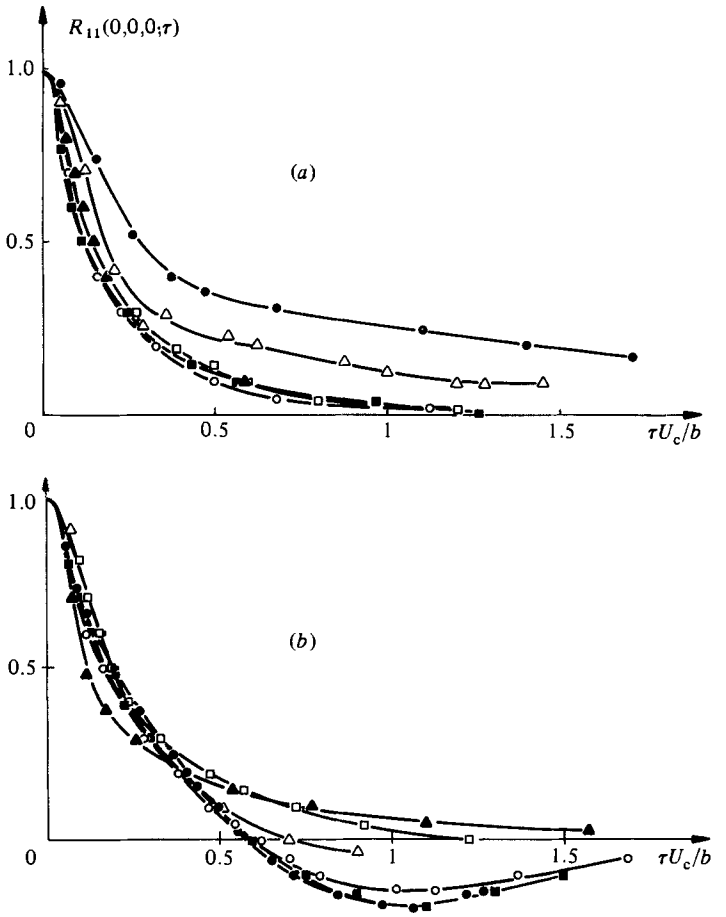

FIGURE 9. Behaviour of the autocorrelation $R_{11}(0, 0, 0; \tau)$. (*a*) On the wake axis: ●, station (*a*); △, (*b*); ▲, (*c*); ○, (*d*); □, (*e*); ■, (*f*). (*b*) At $Y = Y_m$: △, (*a*); □, (*b*); △, (*c*); ○, (*d*); ■, (*e*); ●, (*f*).

deduced from space–time measurements. This point is of interest in the case of supersonic flows because it allows one to overcome some experimental difficulties due to the interaction between probes and prong holders.

Figure 9 shows the results obtained at each test section on the axis of the wake and for $Y = Y_m$. It clearly appears from this figure that the behaviour observed at the first station (*a*) is quite different from that at the other stations; particularly on the axis of the wake (figure 9*a*), the autocorrelation $R_{11}(0, 0, 0; \tau)$ does not reach zero in the time-delay range considered; for values of $\tau U_c/b$ as great as 1.7 the autocorrelation is significantly positive on the axis of the wake at station (*a*). This behaviour is in contradiction with the idea that the typical dimension of coherent structures in a wake is of the order of magnitude of the spatial lateral extension of the flow. This behaviour is also present, though in a less extent, at the second station (*b*) on the axis of the wake. These positive values of $R_{11}(0, 0, 0; \tau)$ might be the consequence of some parasitic effects due to probe vibrations which could result in a positive autocorrelation coefficient; in order to test this interpretation, one can notice that, if there are some parasitic effects due to vibration, these effects should be more perceptible near the region of strong mean velocity gradients ($Y \approx Y_m$) than

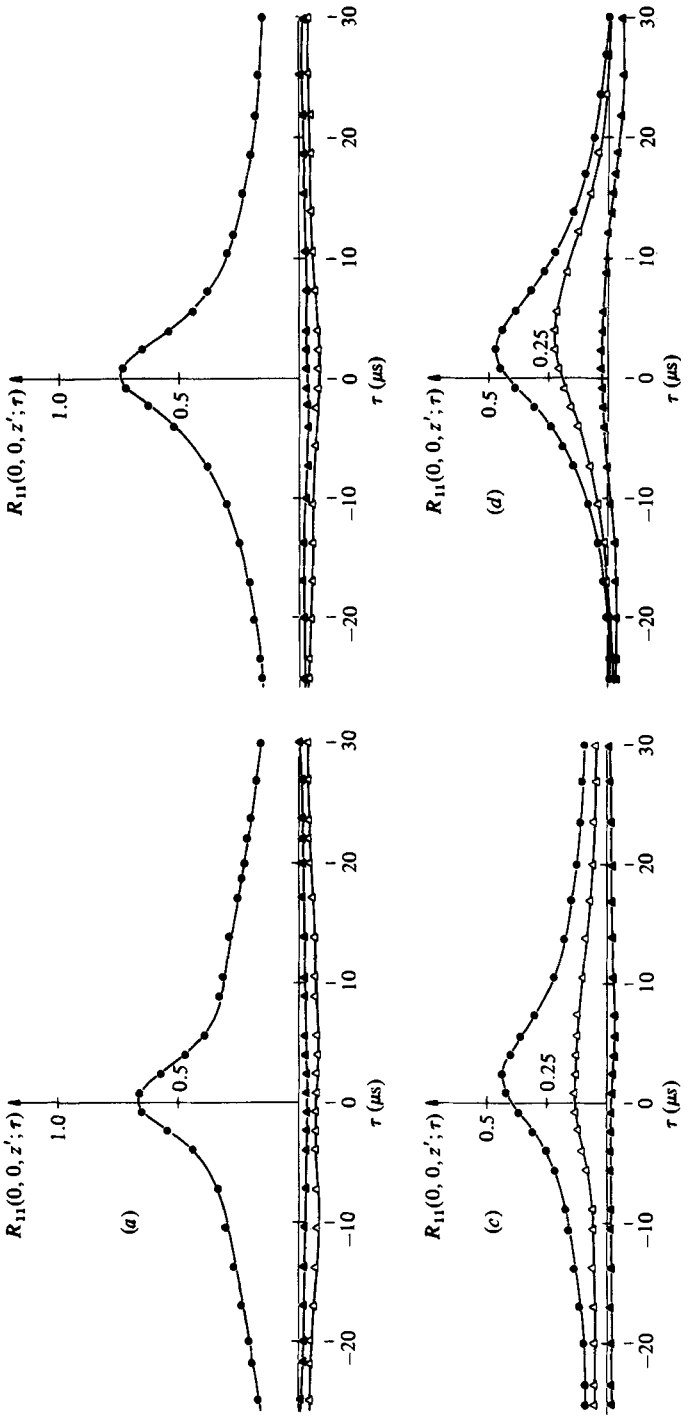

FIGURE 10. Transverse component of space–time correlation $R_{11}(0, 0, z'; \tau)$ at the first two stations. Station (*a*): plot (*a*) on the wake axis and (*b*) at $Y = Y_m$ (●, $z' = 0.36$; △, 0.71; ▲, 1.14). Station (*b*): plot (*c*) on the wake axis and (*d*) at $Y = Y_m$ (●, $z' = 0.23$; △, 0.41; ▲, 0.62).

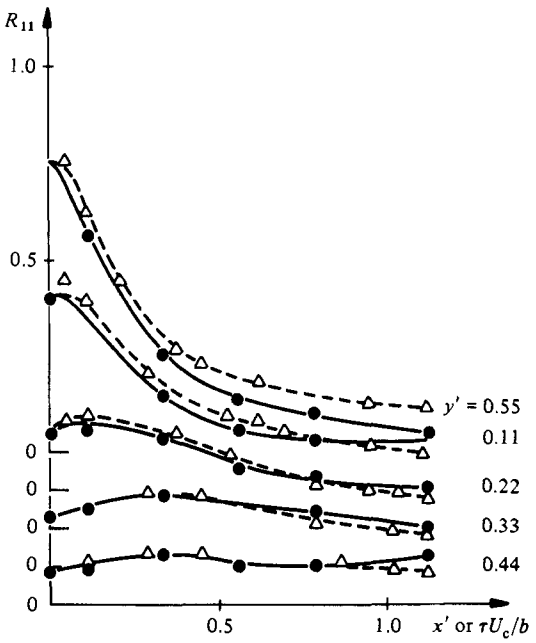

FIGURE 11. Comparison between space and space–time correlations on the wake axis at station (*b*). ●, space correlation $R_{11}(x', y', 0; 0)$; △, space–time correlation $R_{11}(0, y', 0; \tau)$.

on the axis where $\partial U/\partial y = 0$; figure 9(*b*) shows that these effects are not evident at $Y = Y_m$; on the other hand, we have measured space–time correlations between the signals issued from two probes with two different independent holders. In that case figure 10 shows that the space–time correlation $R_{11}(0, 0, z'; \tau)$ also shows significative positive values for large time delay. It appears therefore that the hypothesis of parasitic vibration effects can no longer be retained and that there is a physical phenomenon giving relatively high correlation levels for large time delay.

For $Y = 0$ (on the axis of the wake), the results obtained for stations (*c*)–(*f*) tend monotonicaly towards zero with a satisfactory regroupment of the curves.

When the probe is off the axis, we can also notice that the near-wake stations results do not show the same behaviour as that at the downstream stations. For the last three stations the autocorrelation coefficient $R_{11}(0, 0, 0; \tau)$ reaches large negative values for $\tau U_c/b \approx 1$, and here also the results are quite similar for the three stations.

The comparison between these curves ($R_{11}(0, 0, 0; \tau)$; figures 9*a*, *b*) and the space correlations $R_{11}(x', 0, 0; 0)$, plotted in figure 3, shows that, except at the two stations (*a*) and, to a lesser extent, (*b*), Taylor's hypothesis seems to be valid; however, taking the limitation of the x' domain of figure 3 into account, conclusions on the validity of Taylor's hypothesis cannot be definitively drawn. A more detailed comparison is made by looking at the values of $R_{11}(x', y', 0; 0)$ and $R_{11}(0, y', 0; \tau)$. Figures 11 and 12 show two examples of these comparisons for test sections (*b*) and (*e*).

Finally, the main conclusions regarding the general test of Taylor's hypothesis are: first, at station (*a*) Taylor's hypothesis is clearly not valid, especially on the wake axis; secondly, for all the other stations application of Taylor's hypothesis leads to a relatively good approximation of the space correlations provided that the equivalent distance $x' = \tau U_c/b$ is not too large (typically of order unity) when associated to Y-locations near the outer edge of the wake. These conclusions are in good agreement with the results of Demetriades (1976).

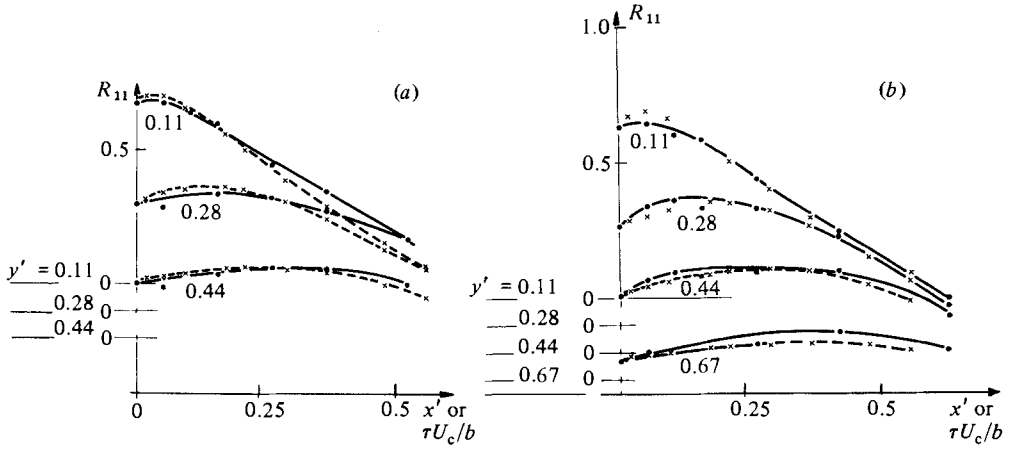

FIGURE 12. Comparison between space and space–time correlations at station (*e*) for $Y = Y_m$ (*a*) and $Y = \frac{1}{2}Y_m$ (*b*): —●—, space correlations $R_{11}(x', y', 0; 0)$; – – × – –, space–time correlations $R_{11}(0, y', 0; \tau)$.

3.3.3. *Spectral distribution*

In order to characterize more precisely the phenomena occuring in the autocorrelation observed at the first station, we perform a frequency analysis of the hot-wire signals.

Figure 13 shows the power-spectral density E^2 plotted as fE^2 versus $\log f$, where f is the frequency. (The areas under the curves directly represent the energy contained between the two limiting frequencies.) The classical description of developed turbulence leads to curves with a unique maximum whose frequency can be evaluated from the mean characteristics of the flow. As an indication, we have plotted the local value of the characteristic frequency $f_c = U_c/b$.

Then, in figure 13 one can observe that, for all the downstream test stations (*b*)–(*f*), the curves have a unique maximum located very near the calculated frequency f_c; however, at the first station the presence of a second maximum can be noticed and occurs at a lower frequency (about 8 times lower) than f_c. It appears that, at this first station, an important part of the total turbulent energy is distributed at very low frequencies compared with the guessed typical frequency.

Space-correlation measurements show that rather-energetic low-frequency phenomena are not convected by the mean flow. We have already mentioned the confluence, at the trailing edge, of two statistically independent turbulent boundary layers; so it seems plausible that these two layers give rise to temporal instabilities occurring at low frequencies; these instabilities rapidly disappear when the distance from the trailing edge increases, and when, simultaneously, the statistical connection between the two sides of the wake grows up.

3.3.4. *Optimum space correlation*

The X-evolution of the optimum space correlation shows the departure from the 'frozen-pattern' ideas. Following Dumas *et al.* (1976) we have plotted in figure 14 the attenuation for the maximum space correlation obtained for the optimum time delay τ_0 when the x' separation increases. The similarity parameter $x'/\Lambda_x(\overline{u'^2})^{\frac{1}{2}}/U^2$ (where Λ_x is the integral scale in the X-direction) proposed by Dumas *et al.* is used in this figure. Although the range of variation of the X-separation is too small to give definitive conclusions, one can observe that, for the three stations (*b*), (*c*) and (*d*), the present measurements are in good agreement with the results obtained by several authors in various configurations for subsonic flows and reported by Dumas *et al.*

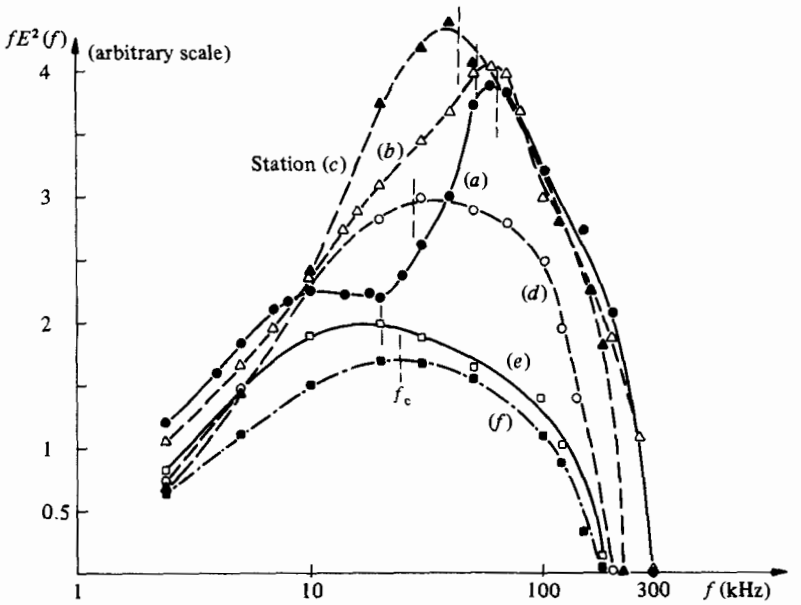

FIGURE 13. Spectral behaviour of the signals; spectral energy $E^2(f)$ versus frequency f; calculated characteristic frequency $f_c = U_c/b$. ●, station (a), $f_c = 64$ kHz; △, (b), $f_c = 51$ kHz; ▲, (c), 45 kHz; ○, (d), 28 kHz; □, (e), 25 kHz; ■, (f), 20 kHz.

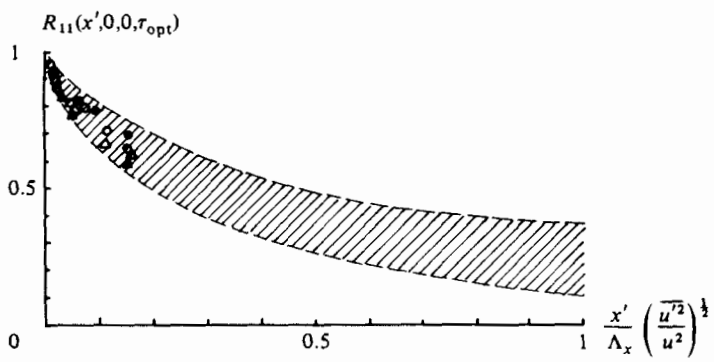

FIGURE 14. Downstream evolution of the optimum space–time correlation $R_{11}(x', 0, 0; \tau \text{ optimum})$. △, station (b), $Y = 0$; ●, (c), $Y = Y_m$; ▲, (e), $Y = Y_m$; ○, (e), $Y = Y_m$. Dashed area: compilation of incompressible-flow measurements after Dumas *et al.* (1976).

3.3.5. *Integral scales*

The analysis of the integral scales gives some additional information concerning the size of the large eddies and their evolution across the flow. These integral scales are defined by

$$\Lambda_{xt} = \frac{U_c}{b}\int_0^\infty |R_{11}(0,0,0;\tau)|\,\mathrm{d}\tau,$$

$$\Lambda_{y^+} = \int_0^\infty |R_{11}(0,y',0;0)|\,\mathrm{d}y',$$

$$\Lambda_z = \int_0^\infty |R_{11}(0,0,z';0)|\,\mathrm{d}z'$$

(y' and z' being always non-dimensional).

Station	(*a*)		(*b*)			(*c*)		(*d*)			(*e*)			(*f*)	
X/θ	19.2		60			108		315			492			709	
Y	0	0.36	0	0.40	0	0.30	0.60	0	0.59	0	0.25	0.50	0	0.50	
$\Lambda_{x\tau}$	—	0.69	0.49	0.28	0.23	0.30	0.26	0.23	0.31	0.25	0.30	0.31	0.21	0.28	
Λ_{y^+}	0.08	0.23	0.13	0.20	0.13	0.19	0.20	0.13	0.25	0.13	0.23	0.25	0.13	0.30	
Λ_z	0.20	0.25	0.27	0.32	0.17	—	0.30	—	—	—	—	0.32	0.25	0.43	
$\Lambda_{x\tau}/\Lambda_{y^+}$	—	3.0	3.8	1.4	1.8	1.6	1.3	1.8	1.2	1.8	1.3	1.2	1.6	0.9	
$\Lambda_{x\tau}/\Lambda_z$	—	2.8	1.8	0.9	1.3	—	0.9	—	—	—	—	0.6	0.9	0.6	

TABLE 2

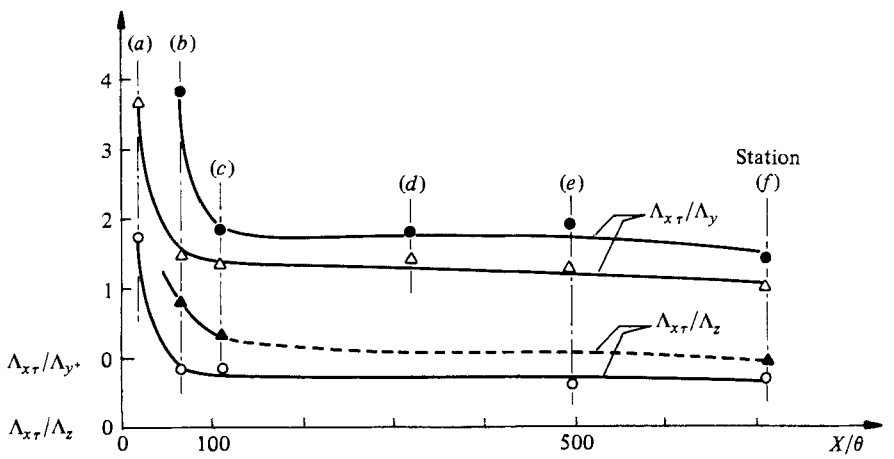

FIGURE 15. Behaviour of integral-scale ratios. Stationary probe on the wake axis (full symbols) or at $Y = Y_m$ (open symbols).

It should be noticed that the insufficient extent of space separations in the y-direction does not allow the calculation of some integral scales such as

$$\Lambda_{y^-} = \int_{-\infty}^{0} |R_{11}(0, y', 0; 0)| \, dy'.$$

Results obtained at each station are given in table 2. One can observe that the scale $\Lambda_{x\tau}$ remains nearly constant between stations (*c*) and (*f*) for a given Y-position; this shows that the dimensional longitudinal integral scale increases in regions II and III at the same rate than b does. It appears also that the integral scale is larger when the probe is located off the axis for every station between (*c*) and (*f*). The transverse scale Λ_{y^+} appears to be nearly constant on the axis of the wake, and also increases at each station when the probe is moved off the axis. The ratio between $\Lambda_{x\tau}$ and Λ_{y^+} is plotted in figure 15; in this figure a very rapid decrease of this ratio occurring between the two first stations is observed (located in the near-wake region). This decrease is followed by a nearly constant level. The ratio $\Lambda_{x\tau}/\Lambda_{y^+}$ is greater on the axis than off the axis, because the Y-location inside the wake has a greater effect on Λ_{y^+} than on $\Lambda_{x\tau}$. The results obtained in incompressible flows show that, for free shear flows like wakes, the ratio Λ_x/Λ_y is about 1.6 (see e.g. Grant 1958) and greater for boundary layers (3 in the measurements of Grant 1958); then, provided that Taylor's hypothesis is an approximation valid everywhere except on the axis of the first station (*a*), it seems that the ratio Λ_x/Λ_y evolves from values of the order of magnitude of

boundary-layer cases to lower values more representative of free shear flows. Only a few results are obtained for Λ_z (see table 2); here it appears also that the integral scale is greater when the probes are off the axis than when they are on the axis. The ratio $\Lambda_{x\tau}/\Lambda_z$ is plotted in figure 15, and shows a rapid decrease followed by a nearly constant level, as $\Lambda_{x\tau}/\Lambda_{y^+}$ does; the values obtained on the axis are always greater than those obtained off the axis; all the transverse scales seem more sensitive to the distance from the trailing edge than the longitudinal scale is. The values obtained by Grant in a subsonic boundary layer lead to a ratio $\Lambda_x/\Lambda_z \approx 2.6$, and in a subsonic wake the value obtained for this ratio is nearly equal to 1.6.

The combined results show that the order of magnitude of the ratio between transverse and longitudinal scales evolves qualitatively from boundary-layer characteristics towards free-shear-flow classical values.

3.4. *General representation of the correlations*

From all the measured space and space–time correlations, the most-synthetic representation of the results is the plot of the isocorrelation contours. As Taylor's hypothesis is verified for stations from (*c*) to (*f*), the isocontours for $R_{11}(x', y', 0; 0)$ or $R_{11}(0, y', 0; \tau U_c/b)$ and for $R_{11}(x', 0, z'; 0)$ or $R_{11}(0, 0, z'; \tau U_c/b)$ are equivalent. In figures 16–21 we present the contour plots for space–time correlations at each test section. For the first station (*a*), only space correlations are plotted on the axis, owing to the failure of the Taylor's hypothesis at these points.

3.4.1. *In the* (*X*, *Y*)- (*or* ($\tau U_c/b$, *Y*)-) *plane*

On the axis of the wake it is noticeable that the isocontours look like ellipses; except for station (*a*), where the situation is complex, it appears that the shape of the isocontours evolves from station (*b*) down to the last station: the ellipses which are significantly inclined with respect to the wake axis at stations (*b*) and (*c*) slowly tend to be aligned with the *x*-axis at the stations far downstream.

When the stationary probe is placed off the wake axis, the isocontour plots appear to have again elliptic shapes, but the wake axis plays an important role. The curves are stretched near the wake axis (this effect being particularly evident when the stationary probe is placed at $Y \approx \frac{1}{2}Y_m$, stations (*c*) and (*e*) for example, see figures 18 and 20). The large extent of the time delay $\tau U_c/b$ allows to draw the negative parts of the correlation contours in the (*X*, *Y*)-plane. These figures put into evidence the well-organized structure of the space–time correlation in this plane.

3.4.2. *In the* (*X*, *Z*)- (*or* ($\tau U_c/b$, *Z*)-) *and* (*Y*, *Z*)-*planes*

Some 'slices' of isocorrelation plots in the (*X* (or $\tau U_c/b$), *Z*)- and (*Y*, *Z*)-planes can be obtained. For test stations (*a*) and (*b*) there is on the axis (figures 16, 17) a quite different behaviour from the one obtained a the four downstream stations, as can be seen from the existence of negative parts of the correlation in the *Z*-direction, as previously mentioned (the negative values measured being very few, the accuracy is not very good and hence, in figures 16*c*, *d*), we have only indicated the frontier between the positive and negative domains). For these stations, on the axis, the isocontours are very elongated towards the $\tau U_c/b$-axis with a symmetry with respect to the *Z*-axis. A similar behaviour is also found at station (*a*), when the stationary probe is off the axis. These characteristics are in qualitative agreement with the results obtained in boundary-layer measurements for incompressible flows (see e.g. Kovasznay, Kibens & Blackwelder 1970, figure 16*f*).

For the other test sections (stations (*c*), (*e*) and (*f*)), the lateral isocontour plots

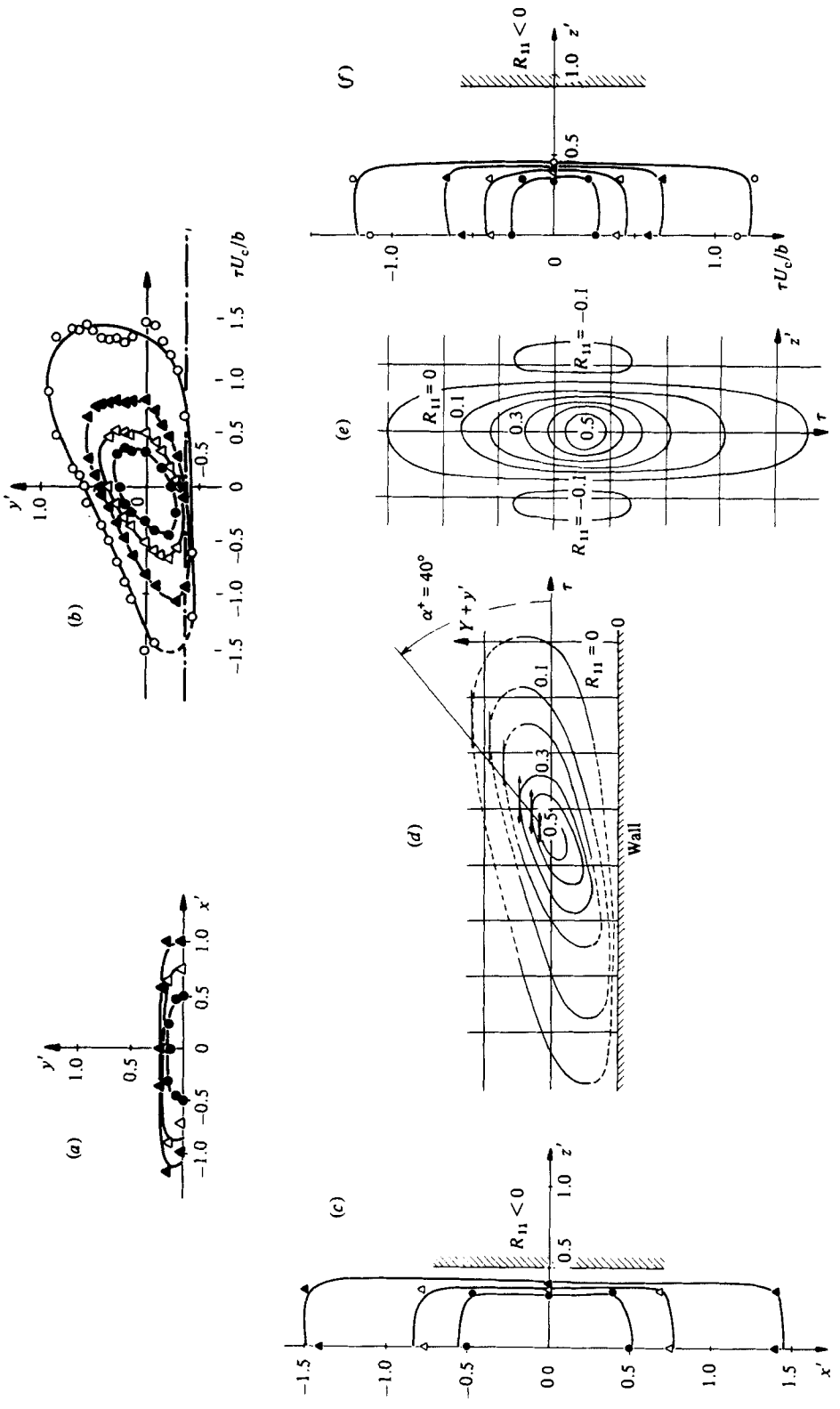

FIGURE 16. Isocorrelation contour plots at station (*a*). In the (X, Y)-plane: (*a*) on the wake axis, $R_{11}(x', y', 0; 0) = 0.1$ (▲), 0.15 (△), 0.2 (●); (*b*) at $Y = Y_m$, $R_{11}(0, y', 0; \tau) = 0.1$ (○), 0.2 (▲), 0.3 (△), 0.4 (●). In the (X, Z)-plane: (*c*) on the axis, $R_{11}(x', 0, z'; 0) = 0.2$ (▲), 0.3 (△), 0.35 (●); (*f*) at $Y = Y_m$, $R_{11}(0, 0, z'; \tau) = 0.2$ (○), 0.3 (▲), 0.4 (△), 0.5 (●). Dashed areas correspond to the negative part of the correlation on plots (*e*) and (*f*). Incompressible boundary-layer results from Kovasznay *et al.* (1970) (arbitrary scale): (*d*) in the (X, Y)-plane; (*e*) in the (X, Z)-plane.

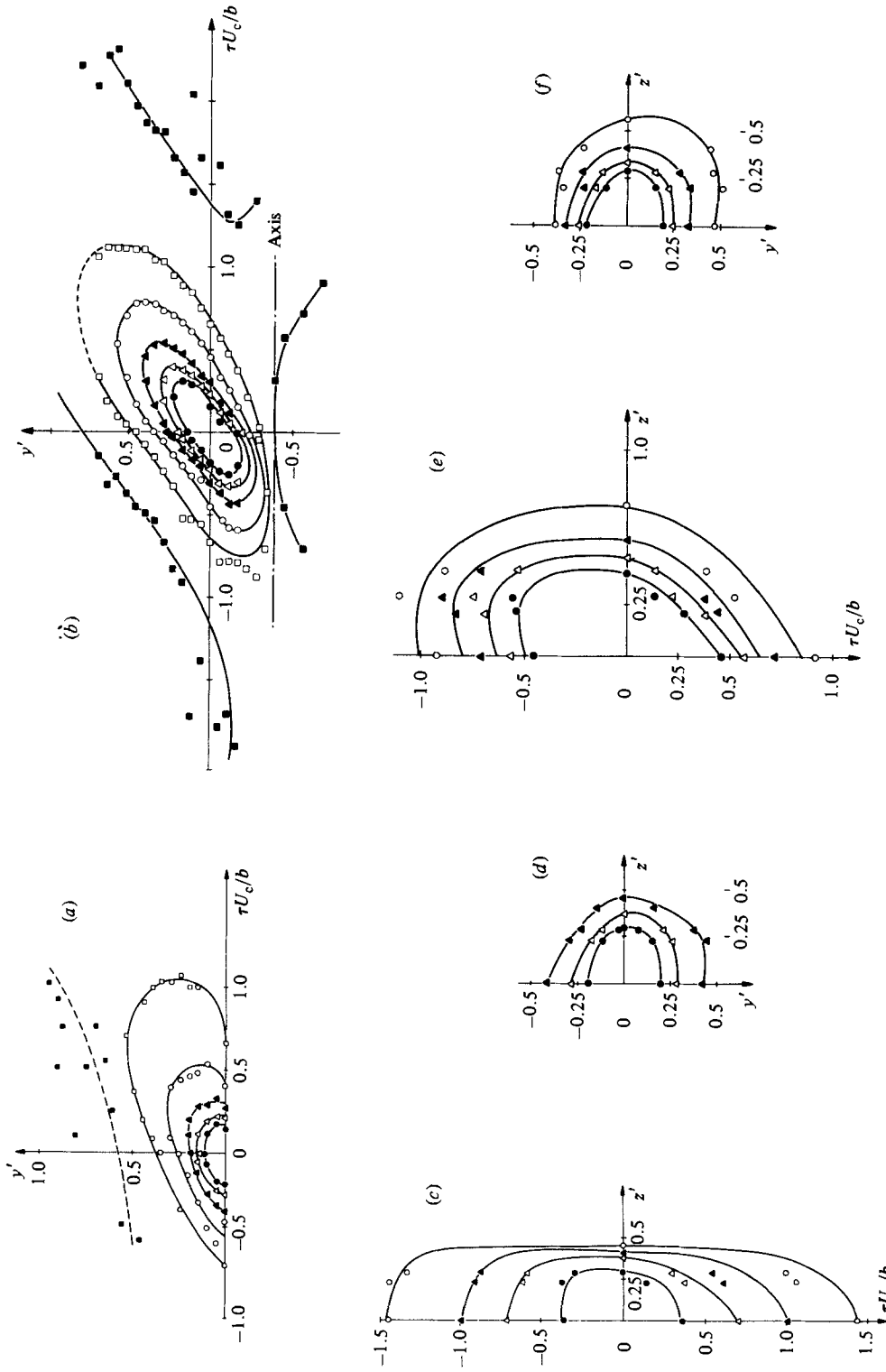

FIGURE 17. Isocorrelation contour plots at station (*b*). In the (X, Y)-plane; (*a*) on the wake axis; (*b*) at $Y = Y_m$, $R_{11}(0, y', 0; \tau) = 0$ (■), 0.1 (□), 0.2 (○), 0.3 (▲), 0.4 (△), 0.5 (●). In the (X, Z)-plane; (*c*) on the axis, $R_{11}(0, 0, z'; \tau) = 0.1$ (○), 0.15 (▲), 0.2 (△), 0.3 (●); (*e*) at $Y = Y_m$, $R_{11} = 0.05$ (○), 0.1 (▲), 0.15 (△), 0.2 (●). In the (Y, Z)-plane; (*d*) on the axis, $R_{11}(0, y', z'; 0) = 0.1$ (▲), 0.2 (△), 0.3 (●); (*f*) at $Y = Y_m$, $R_{11} = 0.1$ (○), 0.2 (▲), 0.3 (△), 0.4 (●).

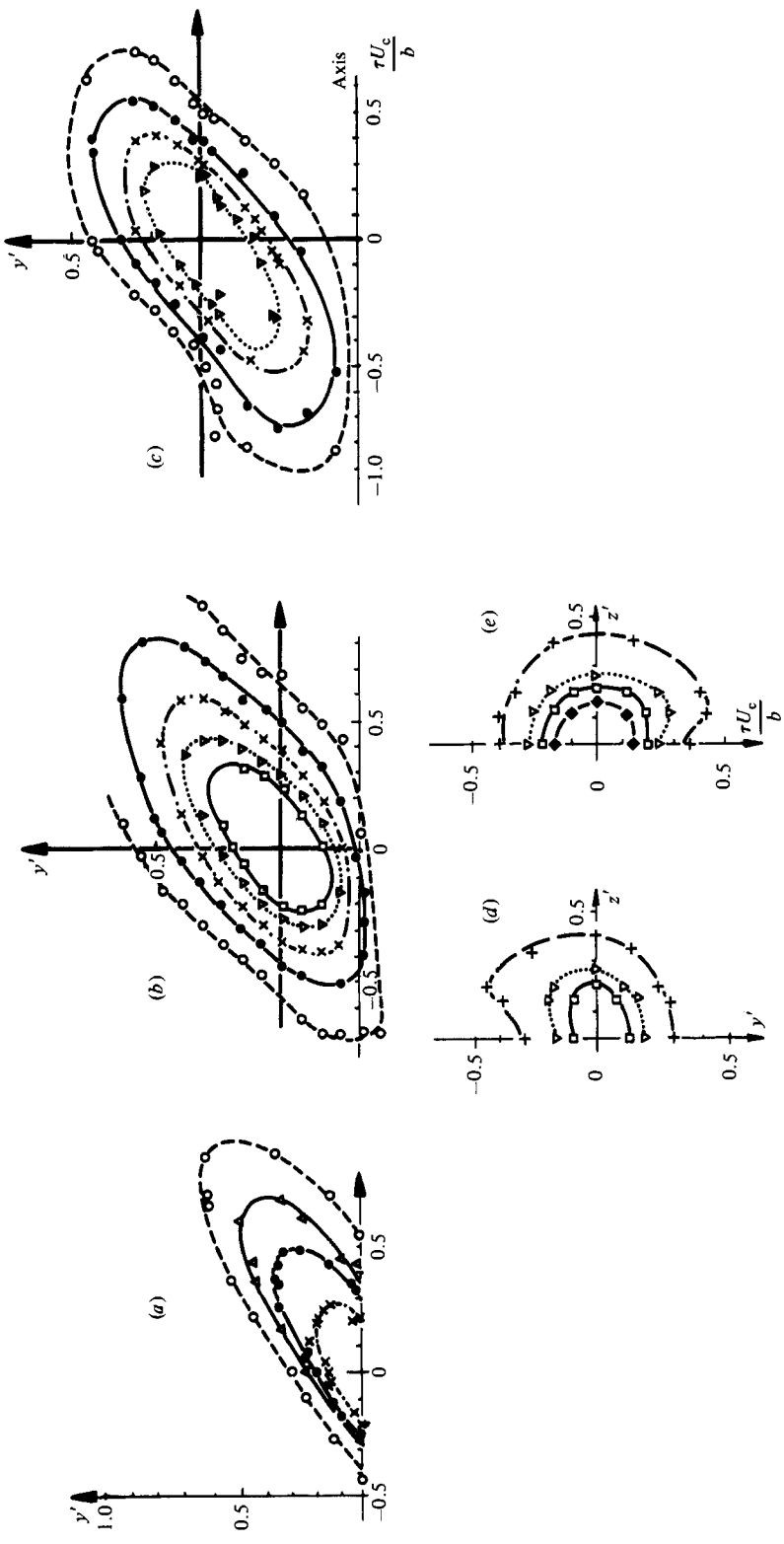

FIGURE 18. Isocorrelation contour plots at station (c). In the (X, Y)-plane; (a) on the wake axis; (b) $Y = \frac{1}{2}Y_m$; (c) at $Y = Y_m$. In the (Y, z)-plane: (d) at $Y = Y_m$. In the (X, Z)-plane: (e) at $Y = Y_m$. $R_{11}(0, y', z'; \tau) = 0.1$ (○), 0.15 (▲), 0.2 (●), 0.25 (+), 0.3 (×), 0.4 (▽), 0.5 (□), 0.6 (◆).

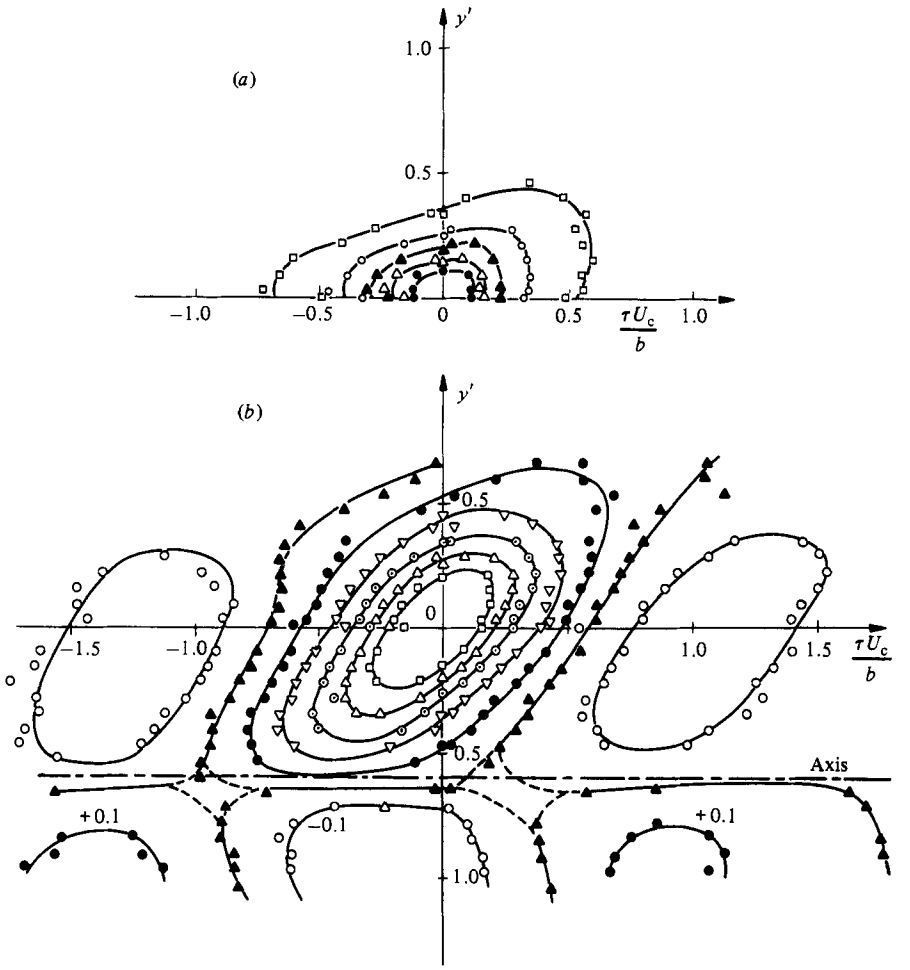

FIGURE 19. Isocorrelation contour plots at station (*d*). In the (X, Y)-plane: (*a*) on the wake axis, $R_{11}(0, y', 0; \tau) = 0.5$ (●), 0.4 (△), 0.3 (▲), 0.2 (○), 0.1 (□); (*b*) at $Y = Y_m$, $R_{11} = 0.5$ (□), 0.4 (△), 0.3 (⊙), 0.2 (▽), 0.1 (●), 0 (▲) and −0.1 (○).

are presented in figures 18, 20 and 21. One can observe that these curves present no symmetry with respect to the Z-axis; a kind of hollow appears in the downstream part of the curves near the plane of symmetry of the wake. This behaviour is observed either in the space-correlation isocontours in the (Y, Z)-plane or in the space–time correlation contours in the ($\tau U_c/b$, Z)-, ((X, Z)-) plane; these two independent sets of correlation-measurement techniques lead to a coherent tridimensional description of the isocorrelation shapes (for the two sets of measurements, the two probes are located at the same X-abscissa, there is then no mutual effect of the probe wakes).

The isocorrelation contour volumes observed from stations (*c*)–(*f*) look like ellipsoids inclined on the wake axis, with a kind of depression on the leeward side near the plane of symmetry of the wake; this description applies in the intermediate wake (region II) and in the developed part of the wake (region III).

3.4.3. *Downstream evolution of the contour plot*

From the previous remarks it appears that the structure of the isocontours evolves gradually from the region near the trailing edge up to the asymptotic part of the wake.

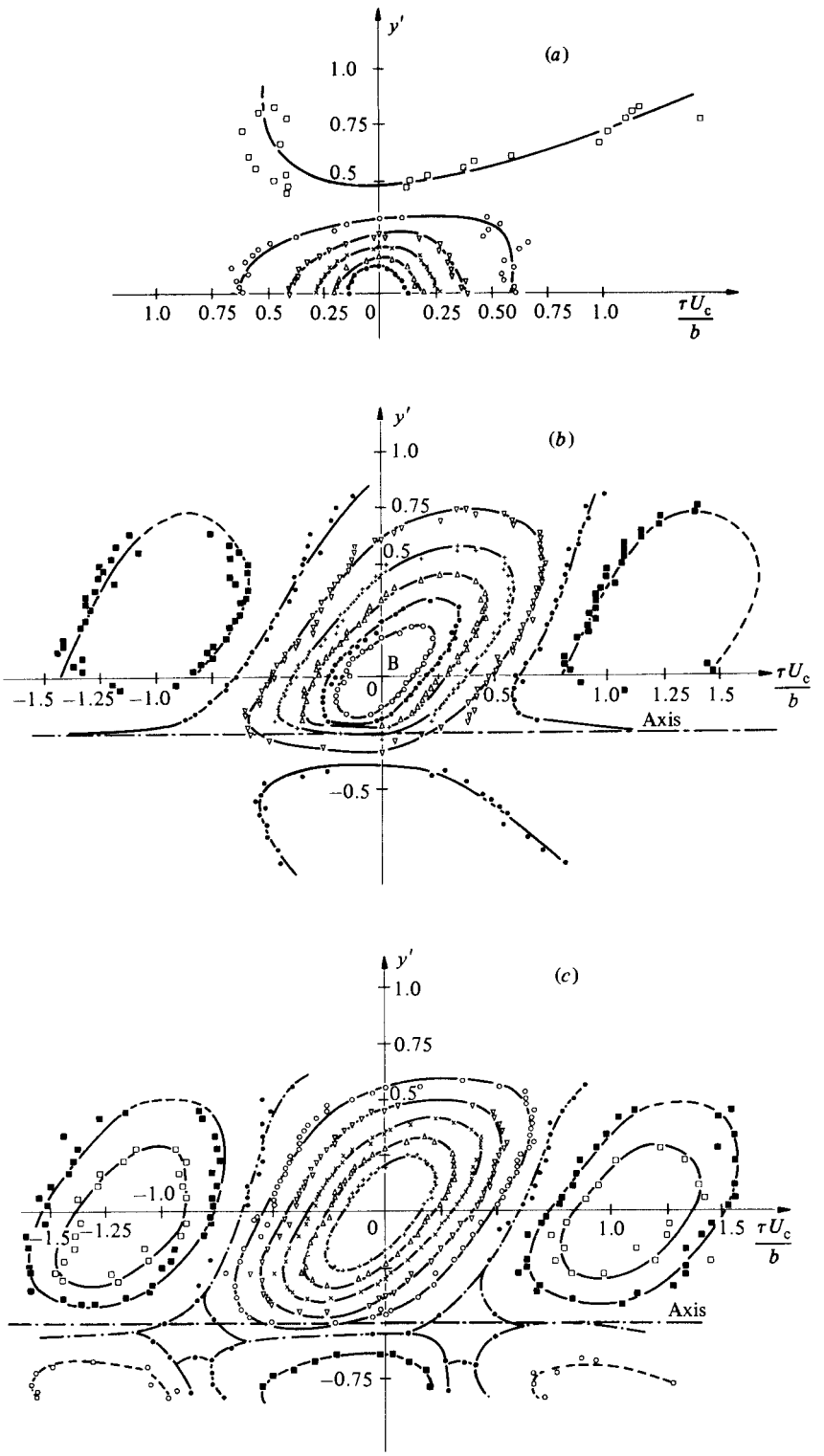

FIGURE 20. For caption see facing page.

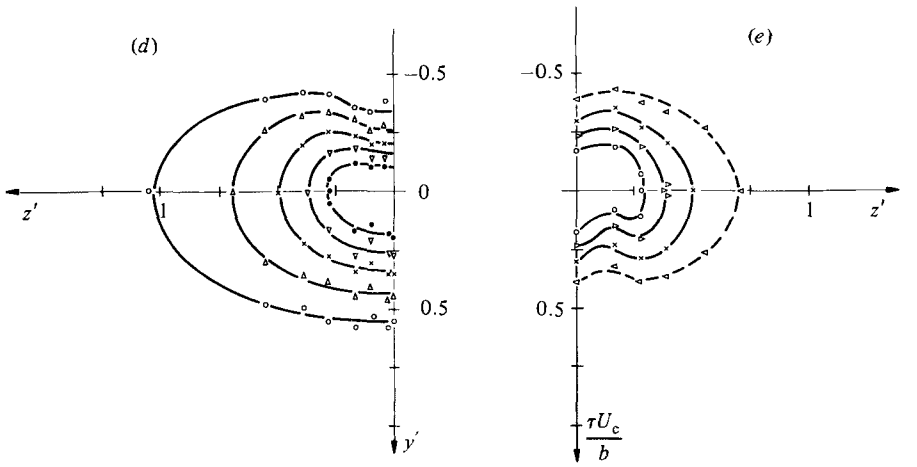

FIGURE 20. Isocorrelation contour plots at station (*e*). In the (X, Y)-plane: (*a*), on the wake axis, $R_{11}(0, y', 0; \tau) = 0.5$ (●), 0.4 (△), 0.3 (×), 0.2 (▽), 0.1 (○), 0.0 (□); (*b*) at $Y = Y_m$, $R_{11} = 0.5$ (○), 0.4 (●), 0.3 (△), 0.2 (+), 0.1 (▽), 0 (●), −0.1 (■); (*c*) at $Y = Y_m$, $R_{11} = 0.5$ (+), 0.4 (△), 0.3 (×), 0.2 (▽), 0.1 (○), 0 (●), −0.1 (■), −0.15 (□). In the (Y, Z)-plane: (*d*) at $Y = Y_m$, $R_{11}(0, y', z'; 0) = 0.5$ (●), 0.4 (▽), 0.3 (×), 0.2 (△), 0.1 (○). In the (X, Z)-plane: (*e*) at $Y = Y_m$, $R_{11}(0, 0, z'; \tau) = 0.5$ (○), 0.4 (▷), 0.3 (×), 0.2 (◁).

A qualitative comparison of the results obtained at the first station near the trailing edge with the measurements of Kovasznay *et al.* (1970) in the case of an incompressible boundary layer is of interest: the overall characteristics are very close together, as shown in figure 16, in the (X, Y)-plane as well as in the (X, Z)-plane. The downstream evolution is characterized by a progressive modification of the inclination angle of the isocontours, when the stationary probe is located off the wake axis.

A more quantitative study can be done by looking at the angle of the ellipse axis with respect to the wake axis. For this purpose, for a given value of space separation y'_0, one can determine the value of time delay τ_0 that maximizes the correlation $R_{11}(0, y', 0; \tau)$; this definition corresponds to the horizontal tangents to the quasi-elliptic curves drawn schematically in figure 22. The X-evolution of the angles α^+ and α^- (defined in figure 22) are plotted on figure 22; one can observe an increase of both angles from the trailing edge up to $X/\theta \approx 400$. The value of α^+ evolves from a value of 45° near the trailing edge up to a mean value of 65° in the asymptotic region. The streamwise evolution of α^- is less important, although quite noticeable.

In the region near the trailing edge, the results obtained in the wake can be compared with several measurements performed in incompressible boundary layers and reported by Dumas *et al.* (1972). As noted by these authors, the effect of decreasing the main velocity gradient is an increase of the angle α^+. We compare in figure 23 the angles obtained here with incompressible boundary-layer results. One can observe that near the trailing edge, the value of α^+ corresponds to the position $Y/\delta \approx 0.5$ (where δ is the conventional boundary-layer thickness), whereas in the asymptotic region the value of the angle is nearly the same as the one obtained in a quasi-homogeneous incompressible flow. When the mean-velocity gradient rapidly decreases from the trailing edge up to the latest part of the wake, the value of α^+ increases, confirming the interpretation of Dumas *et al.* (1972).

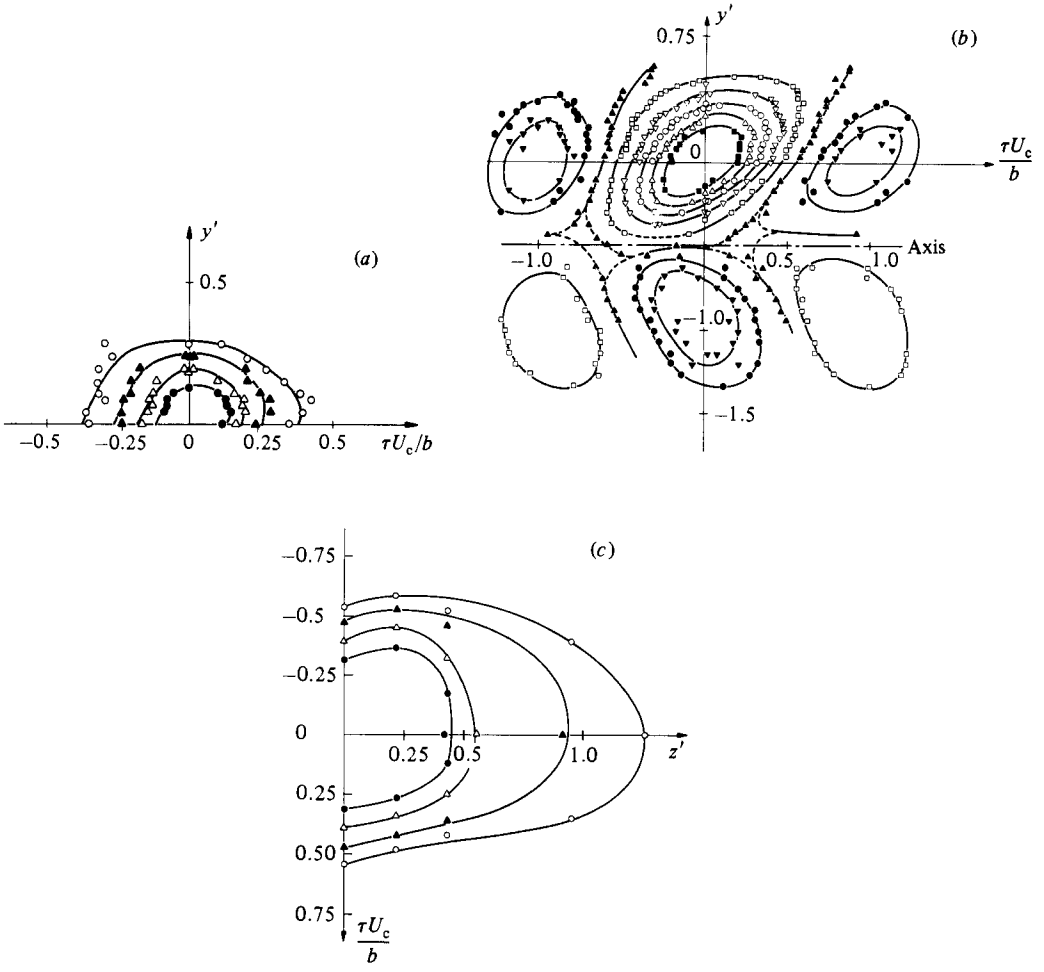

FIGURE 21. Isocorrelation contour plots at station (f). In the (X, Y)-plane: (a), on the wake axis, $R_{11}(0, y', 0; \tau) = 0.5$ (●), 0.4 (△), 0.3 (▲), 0.2 (○); plot (b) at $Y = Y_m$, $R_{11} = 0.5$ (□), 0.4 (△), 0.3 (○), 0.2 (▽), 0.1 (□), 0 (▲), −0.1 (●), −0.15 (▼). In the (X, Z)-plane: (c) at $Y = Y_m$, R_{11} $(0, 0, z'; \tau) = 0.3$ (●), 0.2 (△), 0.1 (▲), 0.05 (○).

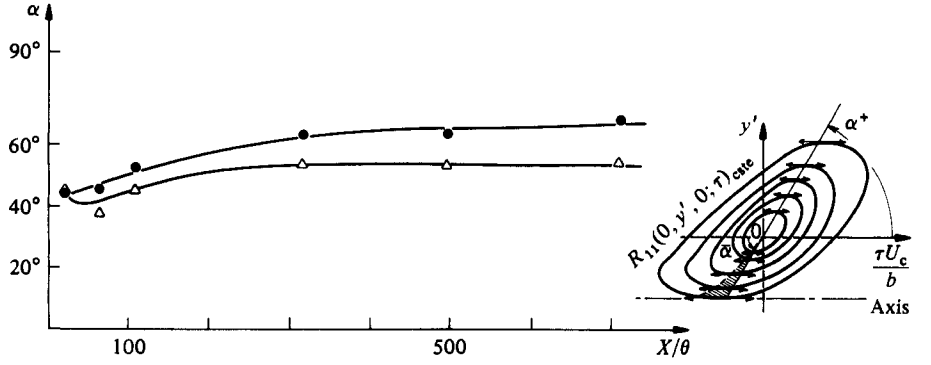

FIGURE 22. Streamwise evolution of the inclination angles α^+ and α^- at the tested stations for $Y = Y_m$. Inclination towards the outer edge of the wake (α^+, ●) and towards the wake axis (α^-, △).

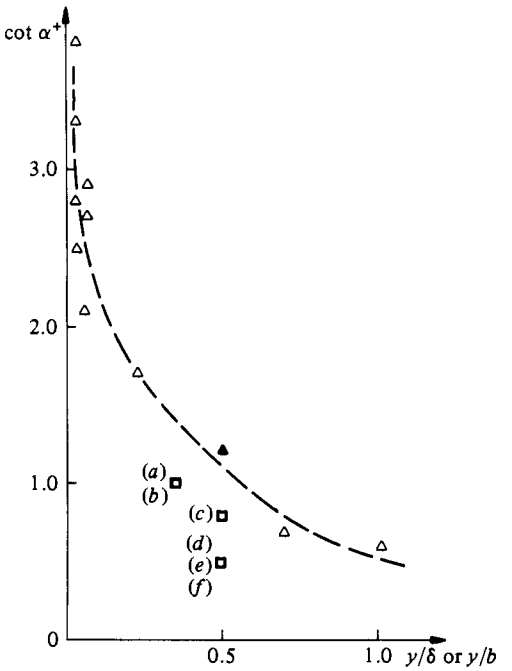

FIGURE 23. Comparison of the evolution of the angle α^+ (see figure 22) for several flows. Incompressible boundary-layer measurements, after Dumas *et al.* (1972) (△) and Kovasznay *et al.* (1970) (▲); and supersonic wake (present results) for the six tested stations from (*a*)–(*f*) (□).

4. Conclusion and prospects

In this paper we have studied a supersonic wake generated by fully developed turbulent boundary layers by means of space and space–time correlations. Despite the large amount of difficulties encountered in any supersonic-flow measurement, we have been able to show a particular evolution from the trailing edge. It appears that the two initially turbulent boundary layers at the trailing edge generate two statistically independent sides of the wake.

The isocontour structures near the trailing edge look like turbulent incompressible boundary-layer ones. In this first stage of the wake development, some temporal instabilities occur and disappear downstream when the developing part of the wake is reached. As the distance from the trailing edge increases, a statistical link between the two parts of the wake builds up progressively.

In the developed part of the wake, all the space and space–time characteristics reach an asymptotic state. In this region the essential features do not agree with the classical results for the incompressible, initially laminar wake behind a cylinder. The usual model of double-roller eddies cannot describe the results obtained here. If one assumes that compressibility does not affect strongly the evolution of moderately supersonic flows, a possible explanation is a memory effect of the situation at the wake's origin. The asymptotic state seems to be dependent on the way the flow is generated, i.e. from laminar or turbulent boundary layers. We shall recall the relative limit of the extent of measurements which can be performed in such a flow; in particular, correlations of transverse components of fluctuating velocities should be of a great help in the complete understanding of the wake behaviour; however, the accuracy of this kind of measurements is at present very questionable (Bestion 1982). Visualizations of this flow will be possible and should give additional informations. On the other hand, equivalent – and more detailed – measurements are needed for

subsonic wakes generated by fully turbulent boundary layers; such results should be of great interest, particularly by allowing comparison with supersonic wakes of the same nature and with initially laminar subsonic wakes.

This research was supported by the Direction des Recherches, Etudes Techniques through Grant 82/169-2.

REFERENCES

BESTION, D. 1982 Méthodes anémométriques par fil chaud: application a l'étude d'intéractions turbulence-gradient de pression élevé en couches limites à vitesse supersonique. Thèse Docteur-Ingenieur, Université Aix-Marseille II, Sept. 1982.

BONNET, J. P. 1982 Etude théorique et expérimentale de la turbulence dans un sillage supersonique. Thèse Doctorat ès Sciences, Université de Poitiers.

BONNET, J. P. & ALZIARY DE ROQUEFORT, T. 1980 Determination an optimisation of frequency response of constant temperature hot-wire anemometers in supersonic flows. *Rev. Sci. Instrum.* **51**, 234–239.

BONNET, J. P. & ALZIARY DE ROQUEFORT, T. 1983 The structure of a two-dimensional, high Reynolds number turbulent wake. In *Structure of complex turbulent shear flow* (ed. R. Dumas & L. Fulachier), pp. 324–333. Springer.

CANTWELL, B. J. 1981 Organized motions in turbulent flow. *Ann. Rev. Fluid Mech.* **13**, 457–515.

DEMETRIADES, A. 1976 Turbulence correlations in a compressible wake. *J. Fluid Mech.* **74**, 251–267.

DUMAS, R., ARZOUMANIAN, E. & FAVRE, A. 1972 Structure de la turbulence: Corrélations spatio-temporelles doubles et triples. *13e Congr. Intl de Méc. Théor. et Appl., Moscou.*

DUMAS, R., FULACHIER, L., ARZOUMANIAN, E. & FAVRE, A. 1976 Etude de la structure de la turbulence dans une couche limite par les corrélations spatio-temporelles. *J. Phys. (Paris)* **37** (C1), 181–184.

FAVRE, A., KOVASZNAY, L. S. G., DUMAS, R., GAVIGLIO, J. & COANTIC, M. 1976 *La Turbulence en Méchanique des Fluides.* Gauthier-Villars.

FINSON, M. L. 1973 Hypersonic wake aerodynamics at high Reynolds numbers. *AIAA J.* **11**, 1137–1145.

FOX, J. 1968 Space correlations measurements in the fluctuating turbulent wakes behind projectiles. *AIAA J.* **6**, 233–238.

GAVIGLIO, J., DUSSAUGE, J. P., DEBIEVE, J. F. & FAVRE, A. 1977 Behaviour of a turbulent flow, strongly out of equilibrium, at supersonic speeds. *Phys. Fluids Suppl.* **20**, S179–S192.

GRANT, M. L. 1958 The large eddies of turbulent motion. *J. Fluid Mech.* **4**, 149–190.

HUSSAIN, A. K. M. F. 1980 Coherent structures and studies of perturbed and unperturbed jets. In *The Role of Coherent Structures in Modelling Turbulence and Mixing* (ed. J. Jimenez). Lecture Notes in Physics, vol. 136, pp. 252–291. Springer.

JAYARAMAN, V. 1983 Etude des corrélations spatio-temporelles dans un sillage turbulent supersonique. Thèse Docteur Ingenieur, Université de Poitiers.

KOVASZNAY, L. S. G., KIBENS, V. & BLACKWELDER, R. F. 1970 Large scale motion in the intermittent region of a turbulent boundary layer. *J. Fluid Mech.* **41**, 283–325.

LAUFER, J. 1975 New trends in experimental turbulence research. *Ann. Rev. Fluid Mech.* **7**, 307–326.

MORKOVIN, M. V. 1956 Fluctuations and hot-wire anemometry in compressible flows. *AGARDograph* **24** (The John Hopkins University, Baltimore).

PAYNE, F. R. & LUMLEY, J. L. 1967 Large eddy structure of the turbulent wake behind a circular cylinder. *Phys. Fluids Suppl.* **10**, S194–S196.

POT, P. J. 1979 Measurements in a 2-D wake and in a 2-D wake merging into a boundary layer. *Data Rep. NRL TR* 79063 L.

RAMAPRIAN, B. R. & PATEL, V. C. 1982 The symmetric turbulent wake of a flat plate. *AIAA J.* **20**, 1228–1235.

THOMAS, R. M. 1973 Conditional sampling and other measurements in a plane turbulent wake. *J. Fluid Mech.* **57**, 549–582.

TOWNSEND, A. A. 1956 *The Structure of Turbulent Shear Flow.* Cambridge University Press.

TOWNSEND, A. A. 1970 Entrainment and the structure of turbulent flows. *J. Fluid Mech.* **41**, 13–46.